Detecting spatiotemporal dynamics of global electric power consumption using DMSP-OLS nighttime stable light data

Article *in* Applied Energy · December 2016

DOI: 10.1016/j.apenergy.2016.10.032

Applied Energy 184 (2016) 450–463

Contents lists available at ScienceDirect

Applied Energy

journal homepage: www.elsevier.com/locate/apenergy

Detecting spatiotemporal dynamics of global electric power consumption using DMSP-OLS nighttime stable light data

Kaifang Shi [a,b], Yun Chen [b], Bailang Yu [a,*], Tingbao Xu [c], Chengshu Yang [a], Linyi Li [d], Chang Huang [e], Zuoqi Chen [a], Rui Liu [a], Jianping Wu [a]

[a] Key Laboratory of Geographic Information Science, Ministry of Education, and School of Geographic Sciences, East China Normal University, Shanghai 200241, China
[b] CSIRO Land and Water, Canberra 2601, Australia
[c] Fenner School of Environment and Society, The Australian National University, Linnaeus Way, Canberra 2601, Australia
[d] School of Remote Sensing and Information Engineering, Wuhan University, Wuhan 430079, China
[e] College of Urban and Environmental Sciences, Northwest University, Xi'an 710127, China

HIGHLIGHTS

- The global NSL data were intercalibrated using the MIR method.
- Global EPC at 1 km resolution were modeled from 1992 to 2013.
- The spatiotemporal dynamics of global EPC were analyzed at multiple scales.

ARTICLE INFO

Article history:
Received 31 May 2016
Received in revised form 27 September 2016
Accepted 14 October 2016

Keywords:
Electric power consumption
Spatiotemporal dynamics
Remote sensing
DMSP-OLS
Nighttime light

ABSTRACT

The rapid development of global industrialization and urbanization has resulted in a great deal of electric power consumption (EPC), which is closely related to economic growth, carbon emissions, and the long-term stability of global climate. This study attempts to detect spatiotemporal dynamics of global EPC using the Defense Meteorological Satellite Program's Operational Linescan System (DMSP-OLS) nighttime stable light (NSL) data. The global NSL data from 1992 to 2013 were intercalibrated via a modified invariant region (MIR) method. The global EPC at 1 km resolution was then modeled using the intercalibrated NSL data to assess spatiotemporal dynamics of EPC from a global scale down to continental and national scales. The results showed that the MIR method not only reduced the saturated lighted pixels, but also improved the continuity and comparability of the NSL data. An accuracy assessment was undertaken and confined that the intercalibrated NSL data were relatively suitable and accurate for estimating EPC in the world. Spatiotemporal variations of EPC were mainly identified in Europe, North America, and Asia. Special attention should be paid to China where the high grade and high-growth type of EPC covered 0.409% and 1.041% of the total country area during the study period, respectively. The results of this study greatly enhance the understanding of spatiotemporal dynamics of global EPC at the multiple scales. They will provide a scientific evidence base for tracking spatiotemporal dynamics of global EPC.

1. Introduction

Electric power consumption (EPC) is indispensable to modern society, playing an important role in supporting socioeconomic development and human life [1–4]. As such, EPC is often one of the main sources of carbon emissions which are the important sources to drive and accelerate global warming [5–8]. After World War II, the world has entered a rapid development stage of industrialization and urbanization. Global EPC showed a massive increase of about four fold from 4512 billion kW h in 1971 to 21, 725 billion kW h in 2012 [9]. This rapid growth is not only closely related to the world energy market and global sustainable development, but also affects the long-term stability of global climate. Hence, accurately and reliably detecting spatiotemporal dynamics of global EPC is crucial for understanding both the impacts and the mechanisms of EPC and its interactions with socioeconomic activities and the environment.

Previous studies have detected spatiotemporal dynamics of EPC in several ways. For example, Ranjan and Jain [10] modeled

* Corresponding author.
E-mail address: blyu@geo.ecnu.edu.cn (B. Yu).

http://dx.doi.org/10.1016/j.apenergy.2016.10.032

spatiotemporal dynamics of EPC in Delhi using linear multiple regression models. Tso and Yau [11] used regression analysis, decision tree and neural networks for the evaluation of EPC. Huang et al. [12] used a Grey-Markov forecasting model to estimate the electric power supply and demand in China from 1985 to 2001. Wang et al. [13] analyzed the changes in industrial EPC in China from 1998 to 2007, using a logarithmic mean Divisia index I decomposition method. Bianco et al. [14] presented temporal EPC in Italy from 1970 to 2007. Bildirici et al. [15] evaluated the causality relationship between EPC and economic growth for US, China, Canada and Brazil. However, most of these investigations used statistical EPC data based on administrative units. In spite of their authoritativeness, the statistical EPC data were both time lagging and short of spatial details, which severely limited their usefulness [5]. More importantly, compared with statistical EPC data, detection of spatiotemporal dynamics of EPC at finer scales is a more realistic application. The results are easier to be integrated with other spatial data layers, so as to carry out interdisciplinary studies [5]. Consequently, more efficient ways of detecting spatiotemporal dynamics of EPC at finer scales are urgently demanded.

Satellite remote sensing imagery, such as the nighttime light data obtained by the Defense Meteorological Satellite Program's Operational Linescan System (DMSP-OLS), is an effective proxy for socioeconomic indicators [16–25]. Since nighttime lights can directly reflect economic activity intensity which is closely related to EPC [26–28], the DMSP-OLS data can be integrated with statistical EPC data to capture spatiotemporal dynamics of EPC in detail over larger areas. Previous studies have demonstrated that DMSP-OLS data have a great potential to model EPC. For example, Elvidge et al. [27] firstly found that DMSP-OLS data were highly correlated to statistical EPC data in 21 countries in the mid-1990s. Amaral et al. [29] demonstrated a close correlation between DMSP-OLS data and statistical EPC data in Brazilian Amazonia in 1999. Similarity, Lo [30] gave a logarithmic relationship between DMSP-OLS data and statistical EPC data for 35 Chinese capital cities. Townsend et al. [31] reported a high correlation between DMSP-OLS data and statistical EPC data in Australia from 1997 to 2002. In addition, Chand et al. [32] analyzed spatial characterization of EPC patterns over India using temporal DMSP-OLS data from 1993 to 2002. He et al. [1] built logarithmic regression models between DMSP-OLS data and statistical EPC data to model spatiotemporal dynamics of EPC at county scale in China from 1995 to 2008. Cao et al. [5] proposed a top-down method to estimate pixel-based EPC in China from 1994 to 2009 using DMSP-OLS data, gross domestic product (GDP), and population as the variables. He et al. [33] detected spatiotemporal dynamics of EPC at the sub-county level in China from 2000 to 2008 using DMSP-OLS data. Using DMSP-OLS data, Xie and Weng [34] modeled spatiotemporal dynamics of EPC in urban cores and suburban regions at Chinese cities from 2000 to 2012. Although previous studies have documented the effectiveness of DMSP-OLS data for estimating EPC with varying degree of success, most of these studies focused on national, regional, or city level evaluation. Due to lack of complete statistical EPC data for all countries in the world, what is missing to date is the detailed exploration of DMSP-OLS data for detecting spatiotemporal dynamics of global EPC. It is, therefore, worthwhile to introduce an effective approach for linking incomplete statistical EPC data with DMSP-OLS data so that the spatiotemporal dynamics of global EPC can be modeled accurately and reliably.

There are two other constraints which limit the reliability and accuracy of modeling spatiotemporal dynamics of global EPC using DMSP-OLS data. The first one is pixel saturation of DMSP-OLS data in the urban center of large cities, and the other is the lack of continuity and comparability of the data [35]. Pixel saturation in DMSP-OLS data results from the OLS sensor's low radiometric resolution of six bits. The OLS sensor was designed to detect low-radiance light sources with radiance ranging from 10^{-10} to 10^{-8} W/cm^2/sr/μm under normal operation [36]. Light sources with radiance ranging >10^{-8} W/cm^2/sr/μm, which often exist in the urban center, were all given the digital number (DN) value of 63 in DMSP-OLS data [33]. Consequently, the different radiance of various lights in the center of urban could not be distinguished. In addition, due to lack of in-flight calibration, discrepancies appeared between DN values derived from different satellites for the same year, and abnormal fluctuations appeared in DN values for different years derived from the same satellite [37,38].

To improve the availability of DMSP-OLS data, many studies have attempted to resolve these two constraints. Among these studies, the invariant region method were widely used to intercalibrate the DMSP-OLS data [39]. The essence of this method is to use a small administrative unit as an invariant region to intercalibrate DMSP-OLS data in the broader regions. For example, Elvidge et al. [40] assumed Sicily, Italy as an invariant region to intercalibrate DMSP-OLS data from 1994 to 2008. Similarly, using Jixi as an invariant region, Liu et al. [37] applied second-order regression models to intercalibrate DMSP-OLS data in China from 1992 to 2008. Although these studies solved the discontinuity problem in DMSP-OLS data, they failed to reduce pixel saturation. In addition, Letu et al. [41] presented an invariant region method within some administrative units to remove the saturated pixels of DMSP-OLS data of Japan. Although this study had advantages of correcting the saturated pixels, it could hardly to optimize continuity and comparability of DN values within DMSP-OLS data. Most recently, Wu et al. [42] has defined Mauritius, Puerto Rico, and Okinawa as the invariant regions to some extent reduce pixel saturation and enhance continuity of DMSP-OLS data in the world. However, all the saturation pixels were assigned to a fix value which means that there is no spatial difference across the corrected saturation pixels for each year. In regard to the invariant region method, research questions remain regarding how to not only effectively reduce saturation pixels but also accurately solve the discontinuity problem in DMSP-OLS data.

To address the above deficiencies, this study attempts to detect spatiotemporal dynamics of global EPC using DMSP-OLS data from 1992 to 2013. The objectives are (1) using a modified invariant region (MIR) method for intercalibrating DMSP-OLS data; (2) linking incomplete statistical EPC data with the intercalibrated DMSP-OLS data for constructing global EPC at 1 km resolution; and (3) evaluating spatiotemporal dynamics of EPC from a global scale down to continental and national scales.

This study is organized as follows. Section 2 briefly describes data sources. Section 3 introduces methodology, presenting the methods for intercalibrating DMSP-OLS data, estimating EPC, and evaluating spatiotemporal dynamics of EPC. Section 4 presents the results and discussion, and conclusions are drawn in Section 5.

2. Data sources

The DMSP-OLS data from 1992 to 2013 were obtained from the National Oceanic and Atmospheric Administration's National Geophysical Data Center (NOAA/NGDC). These data include different types of products. The nighttime stable light (NSL) data include lights from country-sides, towns, cities and other sites with persistent lighting and discard ephemeral events such as fires. The DN values of NSL data range from 0 to 63. Data cover an area of −180 to 180 degrees in longitude and −65 to 75 degrees in latitude, at a spatial resolution of 30-arc-second (about 1 km). Therefore, the NSL product was considered as suitable data to detect spatiotemporal dynamics of global EPC in this study. Currently, the NSL data originate from six satellites: F10 (1992–1994), F12 (1994–1999), F14 (1997–2003), F15 (2000–2007), F16

Table 1
Description of the data used in this study.

Data	Data description	Year	Source
NSL	Annual nighttime stable light composite data	1992–2013	NOAA/NGDC (http://www.ngdc.noaa.gov/eog/dmsp/downloadV4composites.html)
RCNL	Global radiance calibrated nighttime light composite data	2006	NOAA/NGDC (http://www.ngdc.noaa.gov/eog/dmsp/download_radcal.html)
Landsat-4/5 TM	Nine images covering five cities: Beijing, Shanghai, Tokyo, Melbourne, and New York	2010	USGS (http://earthexplorer.usgs.gov/)
EPC	Annual statistical data of EPC (10^4 kW h)	1992–2012	World Bank Open Database (http://data.worldbank.org/)
Boundaries	Shapefile of global continents and countries	2013	ESRI Baruch Geoportal (http://www.baruch.cuny.edu/geoportal/)

(2004–2009) and F18 (2010–2013). These satellites have provided a total of 34 annual products over 22 years.

The global radiance calibrated nighttime light (RCNL) data for 2006 downloaded from NOAA/NGDC were used to facilitate pixel saturation correction of the NSL data. Compared with the NSL data, the RCNL data do not exist saturated pixels in the center of urban areas and have a wide range of DN values. Nine scenes of Landsat-4/5 Thematic Mapper (TM) images were obtained from United States Geological Survey (USGS) to evaluate the saturation correction results of the NSL data. In addition, the statistical EPC data for 132 countries around the world were collected from the World Bank Open Database. The global boundary data for continents and countries were extracted from ESRI Baruch Geoportal. A summary of data used in this study is given in Table 1.

3. Methodology

Three main procedures were undertaken to detect spatiotemporal dynamics of global EPC using the NSL data: firstly, intercalibrating the NSL data using the MIR method; secondly, estimating EPC using the intercalibrated NSL data; and thirdly, evaluating spatiotemporal dynamics of EPC from 1992 to 2013 (Fig. 1).

3.1. Intercalibration of the NSL data

Following the invariant region method proposed by Elvidge et al. [40], Wu et al. [42], and Liu et al. [37]. The global NSL data from 1992 to 2013 were intercalibrated via the MIR method. This method involved two aspects: (1) reduction of saturation effect; (2) Correction of discontinuity effect.

3.1.1. Reduction of saturation effect

As saturated lighted pixels in the NSL data severely limit reliability and accuracy of EPC estimation, we first reduced the saturated lighted pixels within the NSL data through four steps.

Firstly, according to the work of Meng et al. [39], we selected Japan as an invariant region. Because Japan experienced a relatively stable socioeconomic development and had a wide spread of DN values within the NSL data, these characteristics could improve the accuracy of intercalibration.

Secondly, the 2006 RCNL data were chosen as the reference image [42]; we extracted the data of Japan from the NSL data and 2006 RCNL data, respectively.

Thirdly, power regression models (Eq. (1)) were developed between the NSL data and 2006 RCNL data of Japan.

$$DN_{Jap}^{ori} = a \times DN_{Jap}^{b} \tag{1}$$

where DN_{Jap}^{ori} is the DN value of the original NSL data of Japan, DN_{Jap} is the DN value of Japan from 2006 RCNL data, a and b are coefficients. The coefficients of these power regression models are listed in Table 2.

Finally, we assumed that the relationship between the NSL data and 2006 RCNL data of the world was similar to that in Japan. The global NSL data were intercalibrated using the following power regression models.

$$DN_{Glo}^{cor} = \left(\frac{DN}{a}\right)^{\frac{1}{b}} \tag{2}$$

where DN_{Glo}^{cor} is the saturation-corrected DN value of the global NSL data, DN is the original DN value of the global NSL data.

3.1.2. Correction of discontinuity effect

The process of reduction of saturation effect solved the problem of pixel saturation, but the inconsistencies in lighted pixels remained unresolved because the NSL data were composed of multiyear and multisatellite data [43]. Referring to the work of Liu et al. [37], we corrected the discontinuity and incomparability of the global NSL data through two steps.

Firstly, to make full use of information derived from two satellites for the same year, we obtained an intra-annual composition of the NSL data using Eq. (3).

$$DN_{(n,i)}^{intra} = \begin{cases} 0 & DN_{(n,i)}^{d} = 0 \text{ or } DN_{(n,i)}^{e} = 0 \\ (DN_{(n,i)}^{d} + DN_{(n,i)}^{e})/2 & otherwise \end{cases} \tag{3}$$

where $DN_{(n,i)}^{intra}$ is the DN value of the ith lighted pixel after the intra-annual composition in the nth year; $DN_{(n,i)}^{d}$ and $DN_{(n,i)}^{e}$ are DN values of the ith lighted pixel from two saturation-corrected NSL data in the nth year. n is the number of years from 1994 to 2007.

Secondly, since the world is undergoing rapid economic development, EPC growth, and urban expansion, we generated an assumption that the DN value of a lighted pixel detected in an early year would not be less than the DN value of a lighted pixel in a later year [35,44]. We also pointed out that since economic recessions, warfare, and disasters could result in population decline and economic regression in some countries, such as Iraq, Afghanistan, and Libya, these uncertainties were very likely to lead to a decrease in brightness of nighttime lights. However, because the nighttime lights in these countries were only a small proportion of the total nighttime lights in the world, we believed this assumption to be workable. Hence, we performed an inter-annual correction by the following equation.

$$DN_{(n,i)}^{inter} = \begin{cases} 0 & DN_{(n+1,i)}^{h} = 0 \\ DN_{(n-1,i)}^{f} & DN_{(n+1,i)}^{h} > 0 \text{ and } DN_{(n-1,i)}^{f} > DN_{(n,i)}^{g} \\ DN_{(n,i)}^{g} & otherwise \end{cases} \tag{4}$$

where $DN_{(n,i)}^{inter}$ is the DN value of the ith lighted pixel after the inter-annual correction in the nth year; $DN_{(n-1,i)}^{f}$, $DN_{(n,i)}^{g}$ and $DN_{(n+1,i)}^{h}$ are DN values of the ith lighted pixel from intra-annual composition NSL data in the $n-1$th, nth, and $n+1$th years. n represent the number of years from 1992 to 2013. Implementing the method as described above, we obtained the intercalibrated NSL data from 1992 to 2013 (Fig. 2).

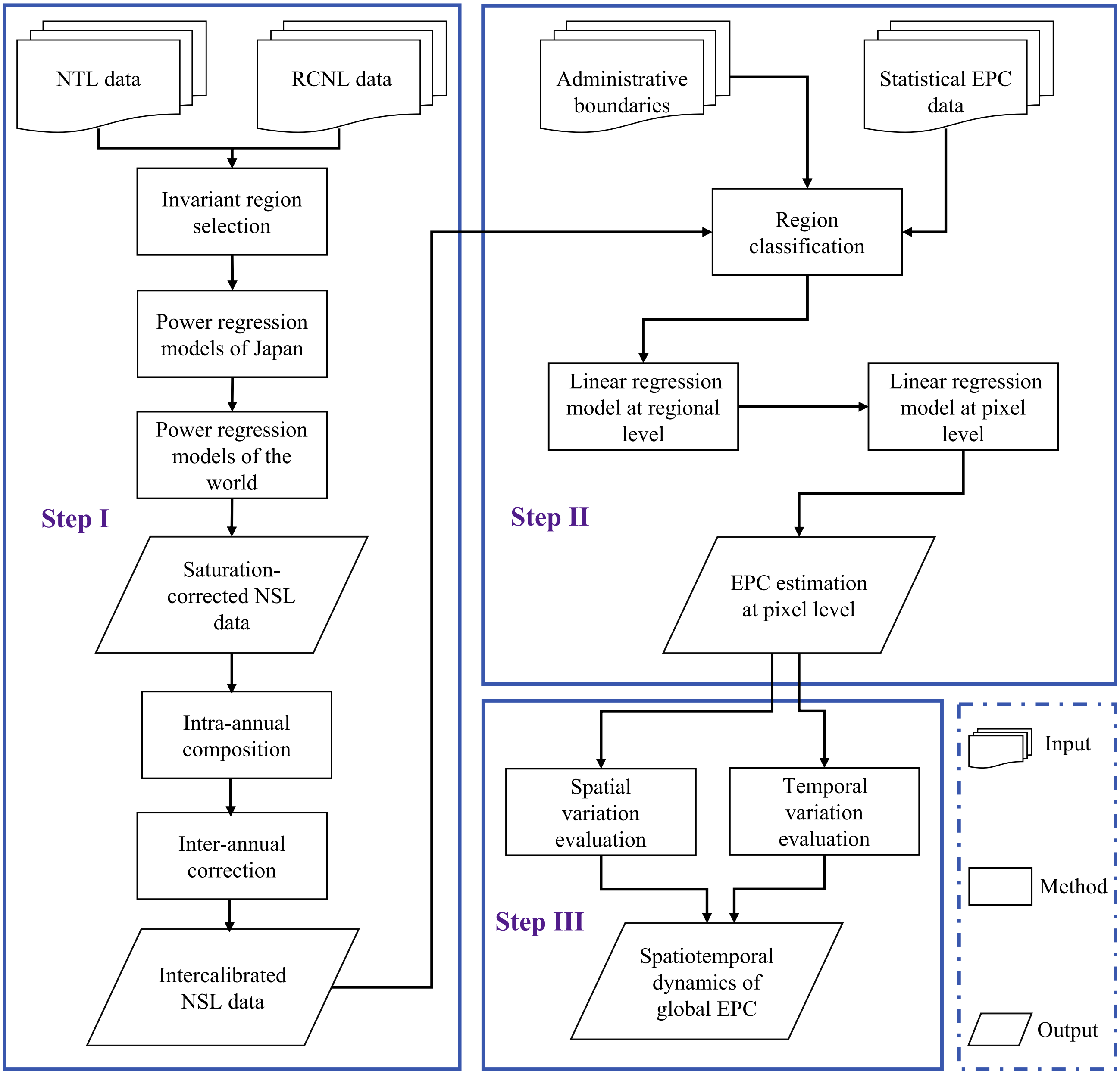

Fig. 1. Flowchart of methodology.

Table 2
Coefficients of the power regression models for saturation correction.

Satellite	Year	a	b	Satellite	Year	a	b
F10	1992	4.665	0.474	F15	2001	5.088	0.464
F10	1993	3.929	0.500	F15	2002	4.865	0.475
F10	1994	4.206	0.493	F15	2003	3.038	0.542
F12	1994	5.111	0.463	F15	2004	3.117	0.543
F12	1995	4.993	0.470	F15	2005	3.539	0.522
F12	1996	5.002	0.470	F15	2006	3.477	0.527
F12	1997	5.148	0.466	F15	2007	3.402	0.530
F12	1998	5.537	0.457	F16	2004	4.297	0.494
F12	1999	6.118	0.439	F16	2005	3.725	0.517
F14	1997	3.958	0.506	F16	2006	3.907	0.509
F14	1998	4.133	0.500	F16	2007	4.567	0.488
F14	1999	4.031	0.505	F16	2008	4.424	0.492
F14	2000	4.131	0.500	F16	2009	4.621	0.480
F14	2001	4.704	0.481	F18	2010	6.497	0.430
F14	2002	4.293	0.496	F18	2011	4.985	0.469
F14	2003	4.113	0.503	F18	2012	5.400	0.461
F15	2000	5.147	0.465	F18	2013	5.400	0.462

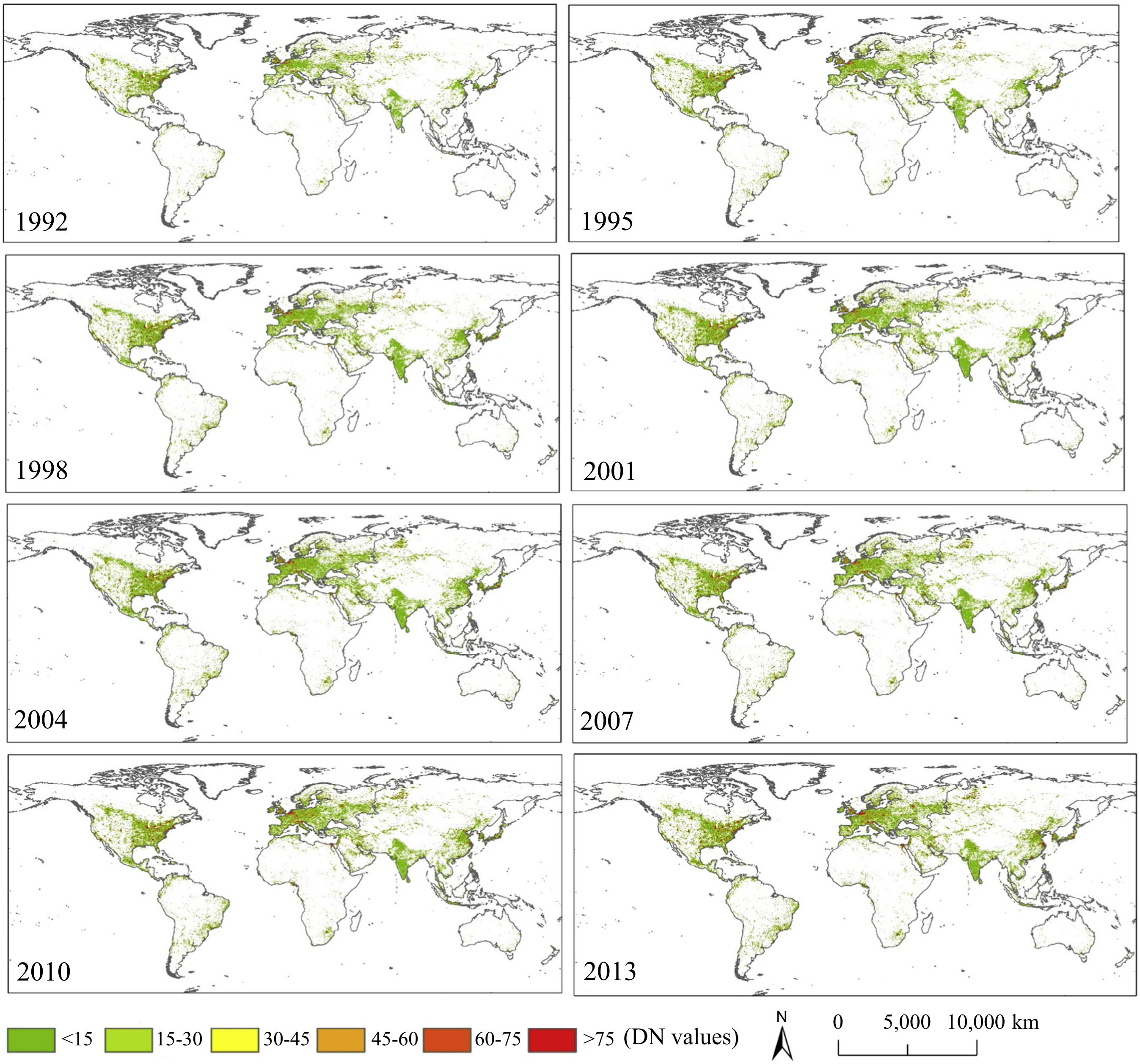

Fig. 2. The intercalibrated NSL data of the world from 1992 to 2013.

3.2. EPC estimation

The estimation of EPC at 1 km resolution using the intercalibrated NSL data was based on a hypothesis that a more developed area generally has brighter lights and higher EPC. In other words, the DN value of a lighted pixel is positively correlated to EPC from the pixel location on the ground. Due to lack of the detailed EPC at the pixel level, we further assumed that the positive correlation between the DN values and statistical EPC was constant within a specific region. Three steps were conducted to accurately estimate global EPC in this study.

Firstly, with the consideration of the regional similarity in geographical location and socioeconomic status, we subdivided the world (264 countries or districts) into 48 regions (Fig. 3).

Secondly, we performed the linear regression model to quantify the correlation between the statistical EPC and intercalibrated NSL data from 1992 to 2012 at the regional scale (Eq. (5)), because the linear regression model was simple with relatively high accuracy, and has been widely applied to EPC estimation [17,33,45,46]. It should be noted that the existing EPC statistics were used to substitute for no data countries in some regions, such as African 7, Asia 12, and South America 1 (Fig. 3).

$$SE_r = cTDN_r \tag{5}$$

where SE_r is statistical EPC in rth region, TDN_r is the total DN value of all the lighted pixels in the intercalibrated NSL data in rth region, and c is coefficient. The coefficients for specific regions are listed in Table 3.

Finally, we used the following Equation to model global EPC with a pixel size of 1 km from 1992 to 2013.

$$E_{ir} = cCDN_{ir} \tag{6}$$

where E_{ir} is estimated EPC of the lighted pixel i in r region, CDN_{ir} is the DN value of the lighted pixel i in r region in the intercalibrated

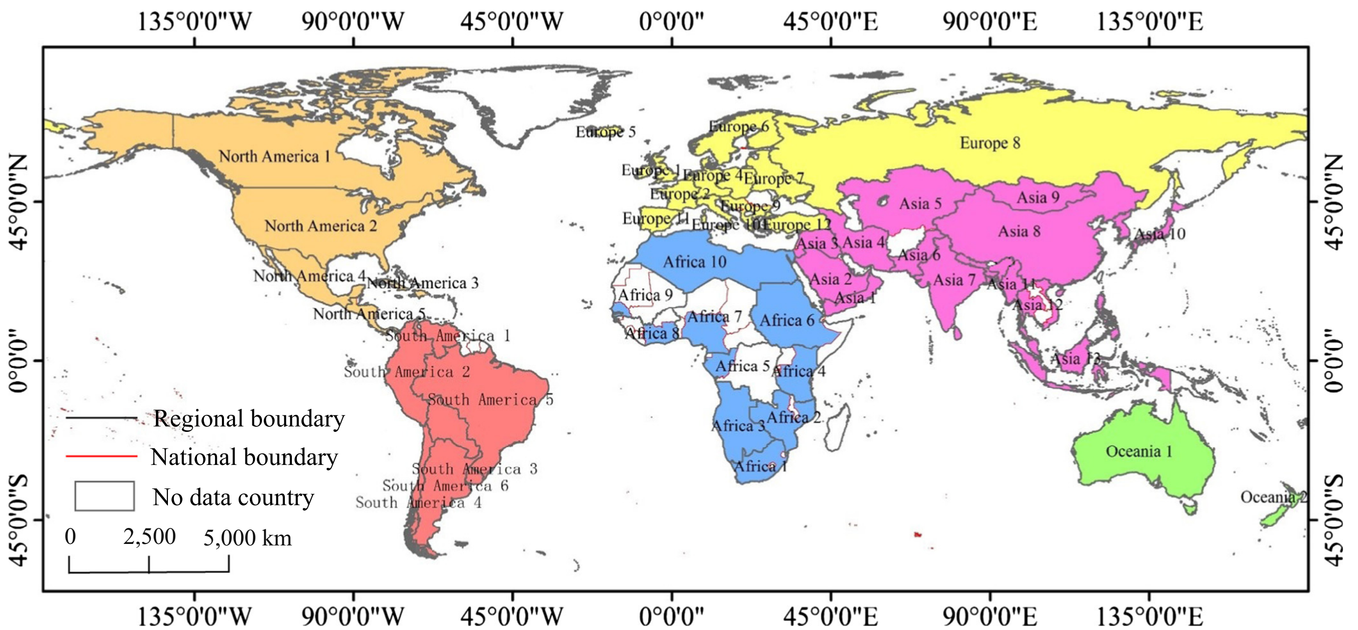

Fig. 3. The classified regions in the world.

Table 3
Coefficients of the linear regression model for EPC estimation.

Region	c	Region	c
North America 1	3.327	Africa 2	5.635
North America 2	3.968	Africa 3	2.361
North America 3	1.599	Africa 4	3.463
North America 4	2.639	Africa 5	0.626
North America 5	2.693	Africa 6	1.547
South America 1	2.617	Africa 7	0.568
South America 2	2.342	Africa 8	2.527
South America 3	1.802	Africa 9	2.789
South America 4	4.717	Africa 10	1.696
South America 5	3.195	Asia 1	1.082
South America 6	2.323	Asia 2	2.619
Europe 1	4.296	Asia 3	2.243
Europe 2	4.804	Asia 4	2.317
Europe 3	7.008	Asia 5	3.317
Europe 4	3.706	Asia 6	2.453
Europe 5	6.618	Asia 7	5.163
Europe 6	3.746	Asia 8	10.415
Europe 7	5.163	Asia 9	5.203
Europe 8	3.250	Asia 10	8.709
Europe 9	5.104	Asia 11	5.659
Europe 10	3.294	Asia 12	5.436
Europe 11	3.236	Asia 13	5.116
Europe 12	5.155	Oceania 1	6.907
Africa 1	6.187	Oceania 2	6.450

NSL data, and c is coefficient determined by regression analysis from Eq. (5). On the basis of the linear regression model and the pixel-based EPC estimation (Eq. (6)), we modeled the annual EPC images in the world from 1992 to 2013 (Fig. 4).

3.3. Evaluation of spatiotemporal dynamics of global EPC

To evaluate the spatial pattern of global EPC, the average EPC from 1992 to 2013 was first calculated with the following Equation:

$$\bar{E}_i = \frac{\sum_{n=1992}^{2013} E_i}{t} \tag{7}$$

where $\bar{E}_i$ is average EPC in pixel i from 1992 to 2013, and t is set to 22 to represent the total number of years.

Then, the Natural Break method [16,47,48] was applied to classify the spatial EPC map. This map was classified into five grades: low (<104 · 10^4 kW h), relatively-low (104–365 · 10^4 kW h), medium (364–741 · 10^4 kW h), relatively-high (741–1399 · 10^4 kW h) and high (>1399 · 10^4 kW h). Note that there were many ways to classify EPC, the Natural Break method was chosen as the purpose here was to investigate statistical variations in different areas, and it provided the smallest variances between categories, without the influence of artificial factors [47,48].

Eq. (8) was then used to describe the temporal variation of global EPC between 1992 and 2013. Again using the Natural Break method, the temporal variation was also classified into five types: no-obvious-growth (<105 · 10^4 kW h), low-growth (105–325 · 10^4 kW h), moderate-growth (325–699 · 10^4 kW h), relatively-high-growth (699–1322 · 10^4 kW h), and high-growth (>1322 · 10^4 kW h).

$$E_i^{tem} = E_i^{2013} - E_i^{1992} \tag{8}$$

where E_i^{tem} is temporal EPC in pixel i between 1992 and 2013.

4. Results and discussion

4.1. Evaluation of NSL data intercalibration

To clearly show the saturation-corrected results of the NSL data, a visual comparison with the finer resolution Landsat-4/5 TM images between the intercalibrated NSL data and original NSL data in year 2010 was undertaken for five metropolises which represented the most developed areas in the world (Fig. 5). Since Wu et al.'s [9] intercalibrated NSL data (Wu's NSL data for short) reduce pixel saturation and enhance DN value continuity of the NSL data to some extent, a comparison with these data was also performing in this study. It has been shown that the presence of saturated lighted pixels constrained the original NSL data to effectively represent urban areas (panel (b) and panel (c)). Although Wu's NSL data relatively improved the ND values in urban centers, the saturated lighted pixels still existed, which also made it difficult to identify urban land use types from nighttime light data (panel (d) and panel (e)). In other words, the saturated lighted pixels in

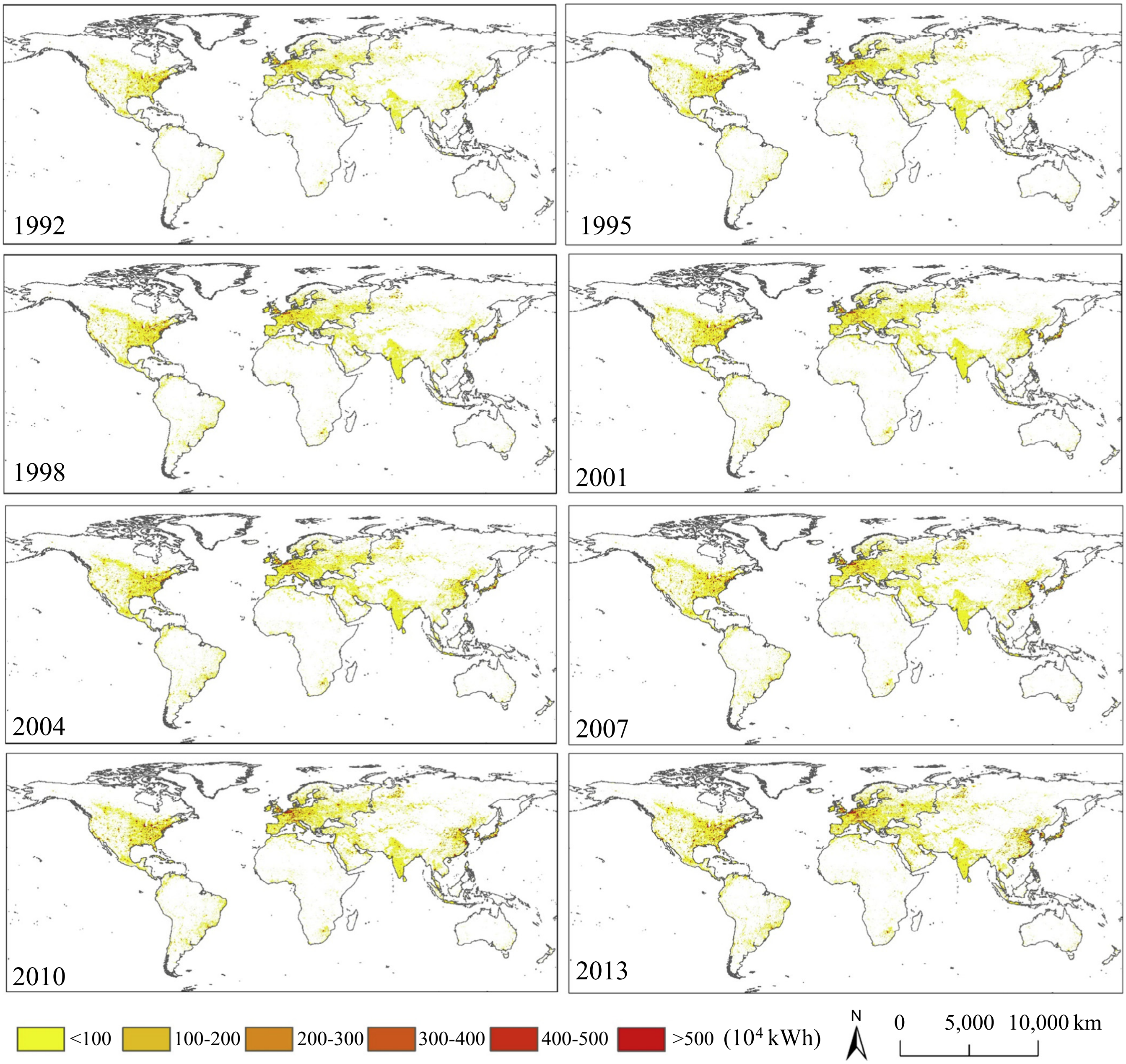

Fig. 4. The estimated EPC in the world from 1992 to 2013 based on the intercalibrated NSL data. Note: the intercalibrated NSL data were resampled to the pixel size of 1 km on Mollweide projection to facilitate calculation.

some metropolises were larger than the actual urban land surface. The intercalibrated NSL data by this study can bring an urban pattern which was much closer to the Landsat-4/5 TM images. The newly intercalibrated data show a clearer distinguish in the transition between urban and suburb areas and improved the differential with urban areas (panel (f)). The saturated lighted pixels have been significantly reduced in urban centers in the NSL data intercalibrated by this study (panel (g)). In summary, the proposed method can effectively reduce the saturated lighted pixels and improve the ability of the NSL data to represent the true human nighttime lights, in particular in the urban areas.

Fig. 6 shows the sums of original and intercalibrated DN values. For the original NSL data, the sum of DN values presents a large gap between two satellites from the same year, while the data derived from the same satellite shows a strong random volatility in inter-annual variability (Fig. 6(a)). Fig. 6(b) illustrates that the sum of DN values of Wu's NSL data presents a relatively stable growth trend. The gap between data for the same year from different satellites has been narrowed, and the abnormal fluctuations of sum of DN values from same satellite in different years have been reduced. However, the discontinuity of Wu's NSL data do not completely disappear. For example, the sum of DN values were 193,496,368 in 1996 from satellite F12 and 185,430,459 in 1997 from satellite F12 (the red[1] block in Fig. 6(b)). Since global EPC has increased rapidly during the last 20 years, nighttime lights have generally increased and such discontinuity seems irrational. Comparing the results with those of original NSL data and Wu's NSL data, the NSL data intercalibrated by this study not only reduced the abnormal

[1] For interpretation of color in Fig. 6, the reader is referred to the web version of this article.

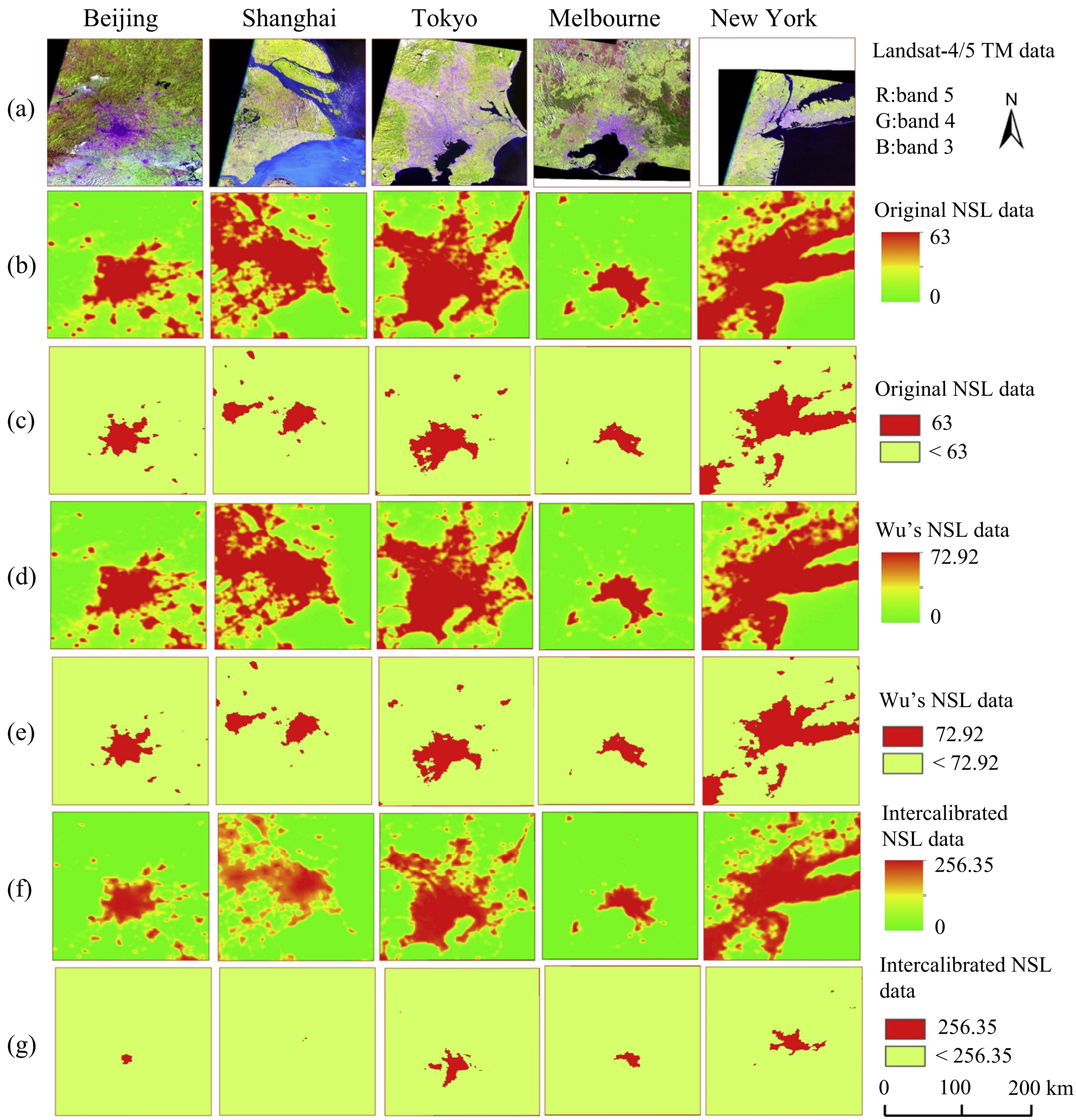

Fig. 5. Comparison of the original NSL data, Wu's NSL data and intercalibrated NSL data for the selected metropolises in reference to the Landsat-4/5 TM data in 2010. Note: all the nighttime light data were resampled to the pixel size of 1 km on Mollweide projection to facilitate comparison.

fluctuations in the sum of DN values for the same satellite over different years, but also removed the discrepancies in the sum of DN values collected from a different satellite for the same year, indicating that our approach helped to produce more consistent annual values which would facilitate the analysis and to draw more reliable results (Fig. 6(c)).

4.2. Accuracy assessment of EPC estimation

The accuracy of global EPC estimation was assessed using country-level statistical EPC. We collected 128 countries' EPC from 1992 to 2012 to calculate EPC for each country from annual EPC images. These countries cover all the developed countries, such as America, Japan, France, and Australia, and most developing countries, such as China, India, Brazil and Mexico. Two indicators were used to evaluate the accuracies of the spatial distributions of global EPC – the coefficient of determination (R^2) and relative error (RE). Table 4 and Fig. 7 show that all the R^2 values were equal to or >0.990 with an average R^2 value of 0.996 for the intercalibrated NSL data, and all the RE values were between −17.663% and 2.635%.

To further evaluate the efficiency of using the intercalibrated NSL to estimate EPC, the original NSL data and Wu's NSL data were also used to estimate EPC in the world, using the same method

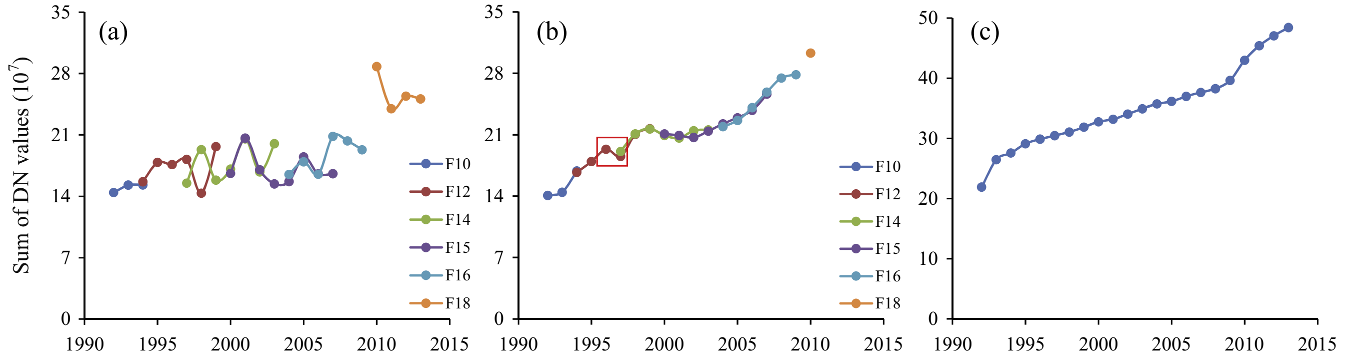

Fig. 6. Sum of DN values in the world: (a) original NSL data from 1992 to 2013; (b) Wu's NSL data from 1992 to 2010; (c) intercalibrated data from 1992 to 2013.

Table 4
Accuracy assessment of the estimated EPC based on the intercalibrated NSL data, original NSL data, and Wu's NSL data.

Year	Statistical EPC (10^8 kW h)	Intercalibrated NSL data			Original NSL data			Wu's NSL data		
		Estimated EPC (10^8 kW h)	RE (%)	R^2	Estimated EPC (10^8 kW h)	RE (%)	R^2	Estimated EPC (10^8 kW h)	RE (%)	R^2
1992	110,413	90,911	−17.663	0.990	114,024	3.271	0.988	93,158	−15.627	0.993
1993	112,376	109,565	−2.502	0.994	120,094	6.867	0.989	95,161	−15.319	0.994
1994	115,219	114,818	−0.348	0.996	122,945	6.705	0.989	112,353	−2.488	0.995
1995	118,908	121,774	2.410	0.997	141,036	18.609	0.987	119,866	0.806	0.997
1996	122,743	125,089	1.912	0.998	139,041	13.277	0.991	127,498	3.874	0.996
1997	125,705	127,942	1.779	0.998	129,048	2.659	0.988	126,490	0.624	0.994
1998	128,498	130,825	1.812	0.997	138,547	7.821	0.982	139,944	8.907	0.994
1999	132,035	134,297	1.713	0.997	139,114	5.361	0.991	143,575	8.740	0.996
2000	137,975	138,122	0.106	0.998	147,801	7.121	0.992	137,857	−0.086	0.995
2001	139,262	140,242	0.703	0.999	144,729	3.925	0.991	136,365	−2.080	0.995
2002	144,175	144,640	0.322	0.998	146,896	1.887	0.990	135,231	−6.204	0.994
2003	149,647	149,425	−0.148	0.998	128,887	−13.872	0.995	141,384	−5.522	0.999
2004	156,412	153,845	−1.641	0.998	135,669	−13.262	0.992	145,218	−7.158	0.996
2005	163,254	155,931	−4.485	0.999	131,788	−19.274	0.997	150,761	−7.653	0.998
2006	169,926	160,274	−5.679	0.999	137,055	−19.344	0.998	159,119	−6.360	0.998
2007	177,936	163,612	−8.050	0.997	148,704	−16.428	0.997	170,421	−4.224	0.995
2008	181,739	167,127	−8.039	0.997	161,450	−11.160	0.997	181,268	−0.260	0.994
2009	180,826	173,561	−4.017	0.993	153,779	−14.957	0.987	183,379	1.412	0.982
2010	193,341	190,282	−1.582	0.994	227,456	17.645	0.991	199,640	3.258	0.983
2011	199,749	201,924	1.089	0.992	189,592	−5.084	0.987	–	–	–
2012	204,230	209,612	2.635	0.990	199,638	−2.248	0.984	–	–	–

described in Section 3.2. The mean R^2 values increased from 0.991, 0.994 to 0.996, whereas the average of absolute RE values decreased from 10.037%, 5.295% to 3.268% after performing the intercalibration for the NSL data in the world (Table 4). Therefore, the intercalibrated NSL data are more suitable for estimating EPC than the original NSL data and Wu's NSL data.

From Table 4, we noticed that the RE values of the intercalibrated NSL data were significantly swung from 1992 to 2012. For example, the RE values were negative from 1992 to 1994. This might be attributed to the corrected errors which resulted in a relatively small sum of DN values in these years. Contrarily, the RE values were positive from 1996 to 2002 which could be attributed to the world's businesses being more and more active in this period, giving it a relatively high nighttime lights. However secondary industries (including manufacturing industry, mining industry, and construction industry) in many countries, especially in the developing countries, was not well developed. As a result, EPC was relatively over-estimated when the intercalibrated NSL data were used as a proxy. In addition, the estimated EPC was generally less than the statistical EPC from 2003 to 2010. During this period, some developing countries, such as China and India, experienced accelerated industrialization and urbanization and consumed considerable amounts of EPC. But these industries and their EPC were hard to detect by nighttime satellite images at nighttime. Additionally, compared with the other years, the sum of DN values from 2011 to 2012 presented rapid growth in the intercalibrated NSL data (Fig. 6(b)), which could lead to a relatively high EPC estimation.

Eight typical countries (United States, Japan, Australia, China, India, Brazil, Bolivia, Mauritius, and Libya) were further used to analyze the accuracy of EPC estimation. In these countries, United States, Japan, and Australia represent the most developed countries; China, India, and Brazil are the rapidly developing countries; Bolivia, Mauritius, and Libya represent less developed countries. Fig. 8 showed that the RE values were relatively low for United States, Japan, and Australia, with a mean of −0.271%, 1.658% and −0.925%, respectively. The primary industries in these countries were finance, commerce, fashion, technology, and culture which were the major sources of EPC, producing bright lights at night. Hence, the use of the intercalibrated NSL data to estimate EPC could result in reliable estimation. Similarly, China, India, and Brazil also possessed accurate EPC estimation (Fig. 8). Chemical industry, manufacturing industry and construction industry were the primary industries in these countries and consumed a large amount of electricity which were hardly monitored by nighttime light images. However, these countries hold a large number of urban population which could give them a relatively higher nighttime lights. To a certain extent, the population lights supplemented

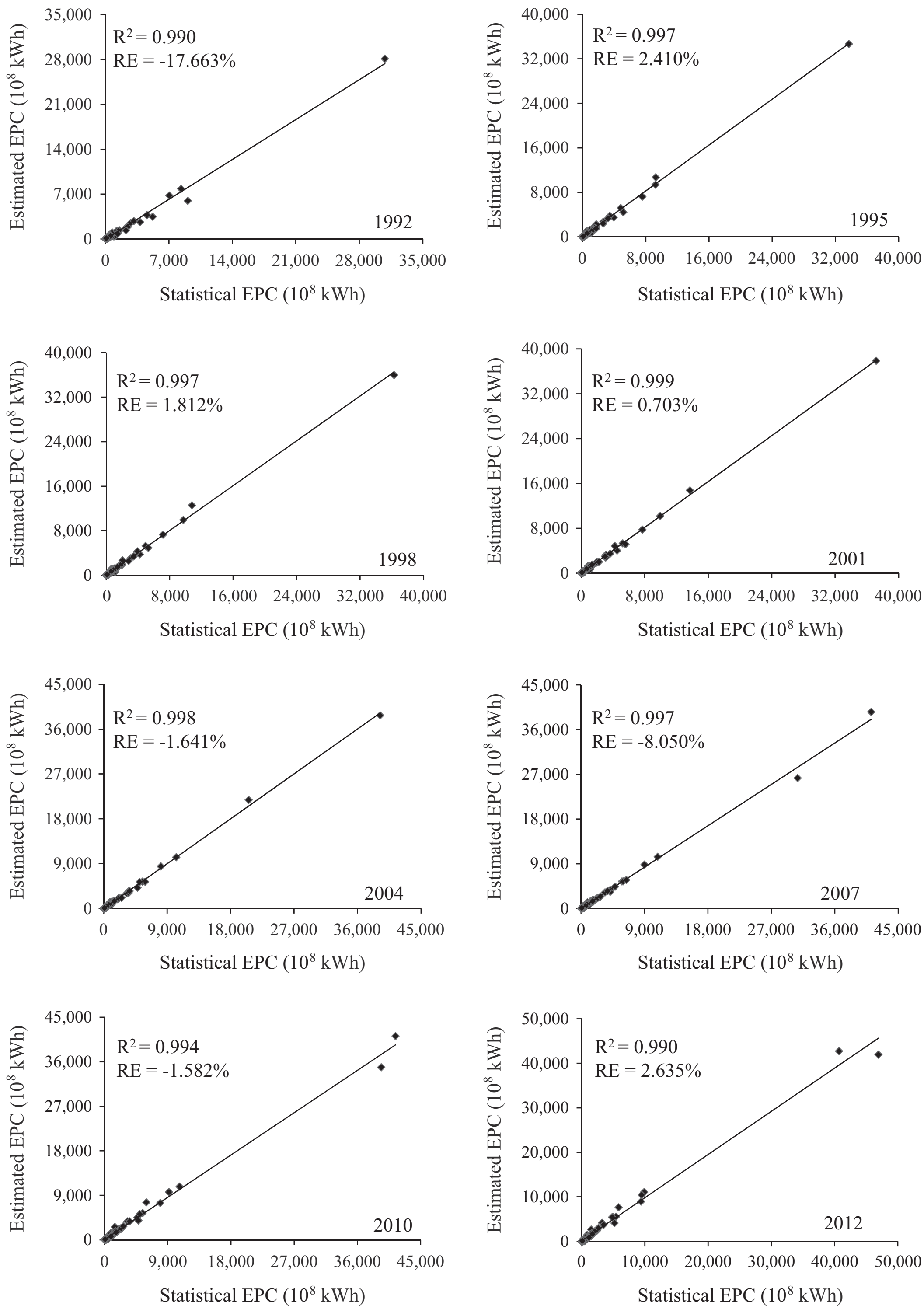

Fig. 7. Accuracy assessment between the estimated EPC and statistical EPC.

the missing lights produced by heavy industries, leading to an accurate estimation. In countries such as Bolivia, Mauritius, and Libya where agriculture is an important industry, EPC was not very high at daytime and nighttime due to the lack of development. But these underdeveloped countries have a relatively high population density in the urban areas, giving them high nighttime lights. Consequently, the EPC was greatly over-estimated in these countries. In summary, because the global EPC was mainly contributed from the developed countries and rapid developing countries, we believe that the intercalibrated NSL data provided a great potential to detect spatiotemporal dynamics of global EPC.

4.3. Spatiotemporal dynamics of EPC from 1992 to 2013

The spatiotemporal dynamics of global EPC from 1992 to 2013 were modeled using the method described in Section 3.3 and results mapped in Fig. 9. During these decades, the spatial variations of global EPC were concentrated in North America, Western

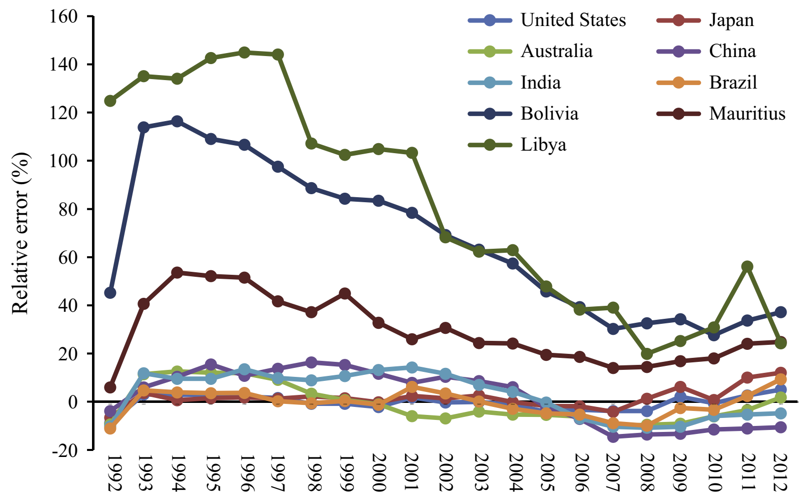

Fig. 8. The relative error values based on the intercalibrated NSL data from 1992 to 2012 for eight typical countries.

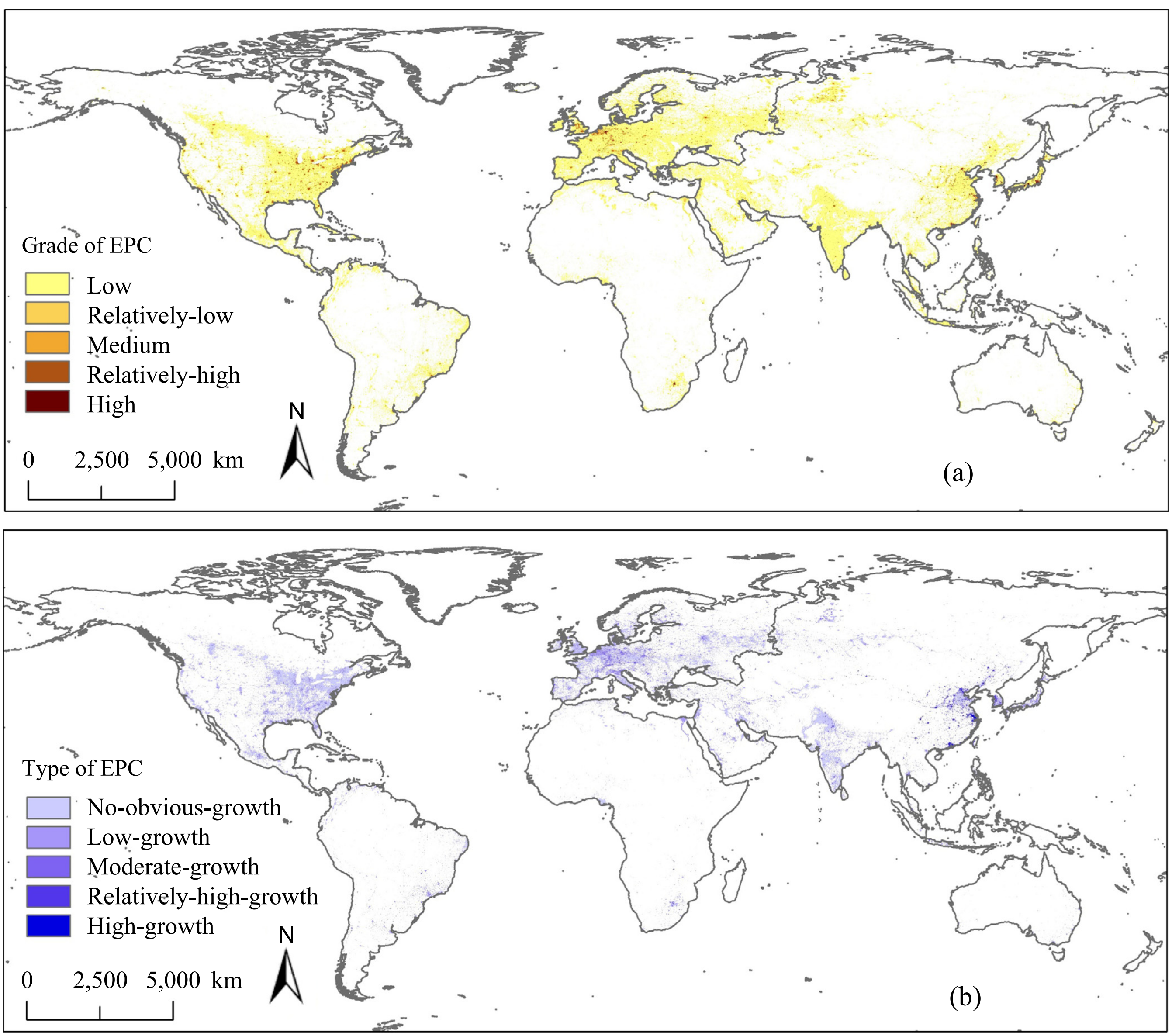

Fig. 9. (a) Spatial variations of EPC in the world and (b) temporal variations of EPC in the world.

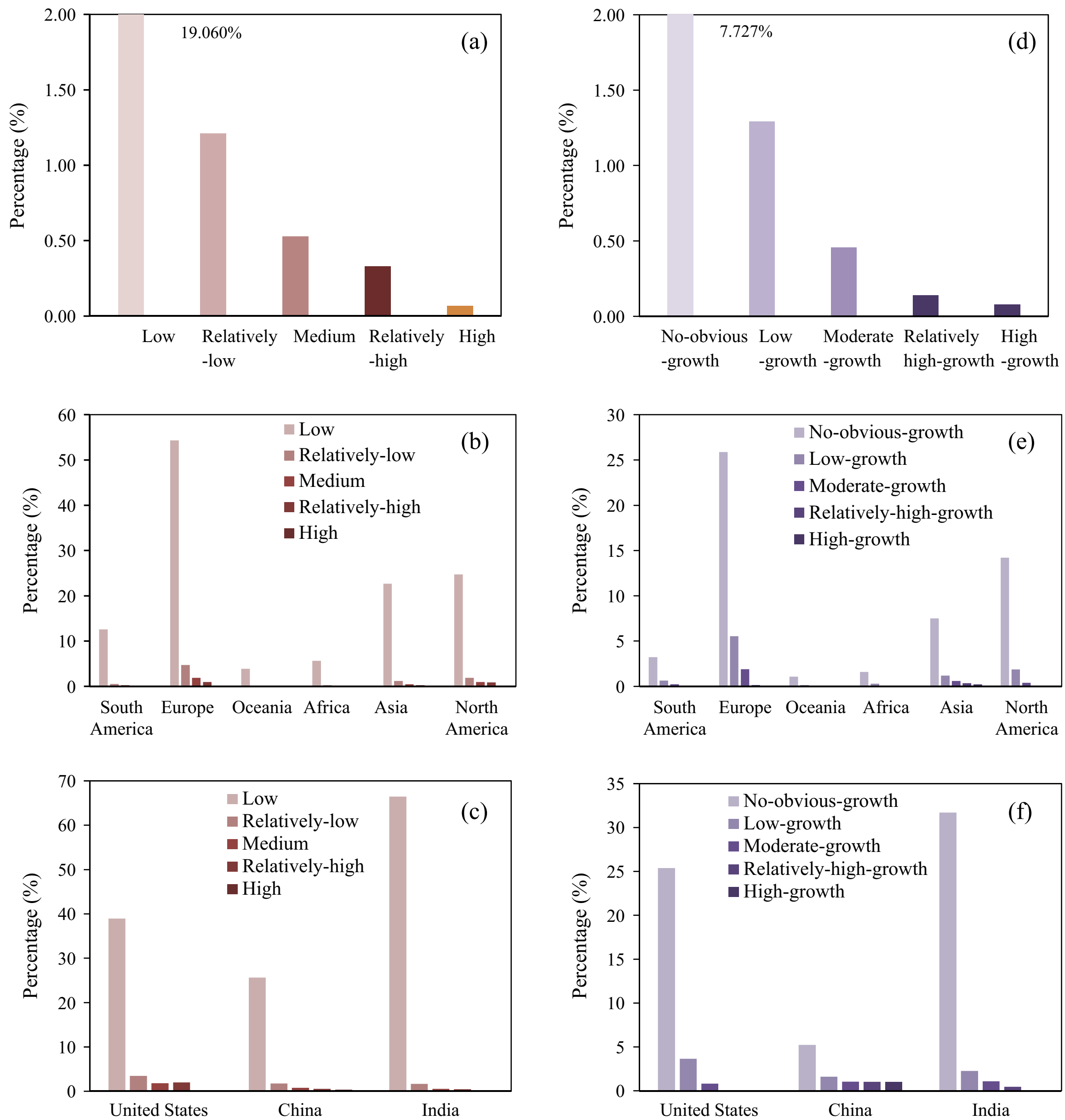

Fig. 10. Areal percentage of each EPC grade at global scale (a), continental scale (b), and national scale (c); areal percentage of each EPC type at global scale (d), continental scale (e), and national scale (f).

Europe, East Asia, and South Asia which have developed socioeconomic conditions or large populations. Contrarily, South America, Africa, and Oceania experienced slight spatial variations of EPC because they had low socioeconomic conditions or relatively small population. To clearly understand the global EPC, we evaluated the spatiotemporal dynamics from a global scale down to continental and national scales.

4.3.1. Spatiotemporal dynamics of EPC at global scale

Fig. 10(a) and (d) plot the five grades and five types of global EPC from 1992 to 2013. Of the total area of the world, the low and relatively-low grades made up 19.060% and 1.210%, respectively. The medium, relatively-high and high grades were mainly distributed in 0.529%, 0.331% and 0.068% of the total area of the world, respectively (Fig. 10(a)). Similarly, the temporal variations of EPC were also mainly located in the metropolitan areas which hold a large population and have undergone rapid urbanization and industrialization. The growth of EPC was concentrated in 9.695% of the total area of the world, with no-obvious-growth, low-growth, moderate-growth, relatively-high-growth, and high-growth accounting for 7.727%, 1.292%, 0.458%, 0.140% and 0.078% of the total area, respectively (Fig. 10(d)).

4.3.2. Spatiotemporal dynamics of EPC at continental scale

Although the world's EPC increased continuously from 1992 to 2013, the differences in amounts and growth rates were huge for the six continents (Fig. 10(b) and (e)). In terms of percentage of total areas, the low, relatively-low and medium grades were 54.300%, 4.739% and 1.897% in Europe, respectively. The relatively-high grade of EPC was 0.980% in Europe and 0.865% in North America. The high grade of EPC was concentrated in Asia, covering 0.165% of its total area (Fig. 10(b)). In addition, the no-obvious-growth type was 25.89% of its total area in Europe whereas this type was much lower in Oceania, Africa, and South America with 1.09%, 1.59%, and 3.21% of their areas, respectively. The growth of EPC was 5.54% in Europe and 1.87% in North America showed a low-growth type, and 0.23% in Asia presented high-growth (Fig. 10(e)). In summary, the spatiotemporal variations of

EPC were mainly identified in Europe, North America, and Asia, with no-obvious variations of EPC found in South America, Africa, and Oceania.

4.3.3. Spatiotemporal dynamics of EPC at national scale

Three countries (United States, China, and India) were selected in this study to clearly evaluate spatiotemporal dynamics of EPC at a national scale. These countries are the largest developed and developing countries in the world, and their economic growth and EPC have greatly impacted global socio-economic changes. Fig. 10(c) and (f) contained the areal percentage of each grade and type in the three countries. The low grade was concentrated in the India and accounted for 66.445% of its total area. Of the total area of United States, the relatively-low, medium and relatively-high grades made up 3.502%, 1.838%, and 1.992%, respectively. It should be pointed out that the high grade was mainly located in China, covering 0.409% of its total area (Fig. 10(c)). In addition, India was dominated by no-obvious-growth type (>30%). Again, the low-growth type was concentrated in America, accounting for 3.654% of its total area. Special attention should be paid to China where the moderate-growth, relatively-high-growth and high-growth covered 1.032%, 1.022% and 1.041% of its total area, respectively (Fig. 10(f)). In summary, the spatiotemporal variations of EPC were mainly identified in China, with no-obvious variations of EPC found in United States and India.

4.4. Limitations and future directions

This study still has a few limitations. For example, the assumption of continuous DN growth could result in overestimations in some countries which have experienced population decline or economic recessions. Improving the reliability of global statistical EPC data would surely increase the accuracy of the method proposed in this study. Future research will focus on the improvement of intercalibrated method to increase EPC estimation accuracy. We will also explore spatiotemporal dynamics of global electric power consumption at the different scales (including county scale, provincial scale, and national scale) and their driving forces which are closely linked to global energy consumption and carbon dioxide emission. In addition, with the release of the first global Suomi National Polar-orbiting Partnership (NPP) Visible Infrared Imaging Radiometer Suite (VIIRS) nighttime light composite data at 0.5 km resolution, further improvement on spatiotemporal dynamics of EPC becomes possible.

5. Conclusions

In response to the rapid EPC increase in the world, this study attempted to detect spatiotemporal dynamics of global EPC using the NSL data from 1992 to 2013. The MIR method was proposed to intercalibrate the global NSL data. The advantages of this method are that it is simply dependent on the power regression models between the NSL data and 2006 RCNL data, and it not only reduces the saturated lighted pixels, but also improves the continuity and comparability of the NSL data in the world from 1992 to 2013. The global EPC at 1 km resolution was modeled using the intercalibrated NSL data. The accuracy assessment demonstrated that the intercalibrated NSL data were relatively suitable and accurate for estimating EPC in the world. The spatiotemporal dynamics of EPC were evaluated from a global scale down to continental and national scales. The model outputs clearly presented the large variations of EPC among different regions. The spatiotemporal variations of EPC were mainly identified in Europe, North America, Asia, and China, with no-obvious variations of EPC in South America, Africa, Oceania, United States, and India.

We consider the proposed intercalibration method to be worthwhile because it improved the reliability of global EPC estimation. Our EPC estimation in the world is valuable because they not only provide global EPC at 1 km resolution, where EPC information has often been difficult to obtain, but also enhance the human activity data content which is an indispensable part of the big data era. In addition, the simulated spatiotemporal dynamics will improve the understanding of regional discrepancies of EPC at the multiple scales, and provide a scientific basis for the effective and sustainable utilization of EPC in the world.

Acknowledgements

This work is supported by the National Natural Science Foundation of China (No. 41471449), the Natural Science Foundation of Shanghai (No. 14ZR1412200), the Innovation Program of Shanghai Municipal Education Commission (No. 15ZZ026), the Fundamental Research Funds for the Central Universities of China, and the China Scholarship Council (No. 201406140007). The authors also wish to thank their colleagues Susan Cuddy for her helpful suggestions. The global electric power consumption datasets are available for download through the website of http://pan.baidu.com/s/1cefAY6.

References

[1] He C, Ma Q, Li T, Yang Y, Liu Z. Spatiotemporal dynamics of electric power consumption in Chinese Mainland from 1995 to 2008 modeled using DMSP/OLS stable nighttime lights data. J Geogr Sci 2012;22:125–36.
[2] Payne JE. A survey of the electricity consumption-growth literature. Appl Energy 2010;87:723–31.
[3] Fanelli V, Maddalena L, Musti S. Modelling electricity futures prices using seasonal path-dependent volatility. Appl Energy 2016;173:92–102.
[4] Kwon S, Cho S-H, Roberts RK, Kim HJ, Park K, Yu T-HE. Short-run and the long-run effects of electricity price on electricity intensity across regions. Appl Energy 2016;172:372–82.
[5] Cao X, Wang J, Chen J, Shi F. Spatialization of electricity consumption of China using saturation-corrected DMSP-OLS data. Int J Appl Earth Obs Geoinf 2014;28:193–200.
[6] Jacobson MZ. Review of solutions to global warming, air pollution, and energy security. Energy Environ Sci 2009;2:148–73.
[7] Lean HH, Smyth R. CO_2 emissions, electricity consumption and output in ASEAN. Appl Energy 2010;87:1858–64.
[8] Lei L, Wang Y, Fang S, Ren C, Liu T, Chen F. Efficient syngas generation for electricity storage through carbon gasification assisted solid oxide co-electrolysis. Appl Energy 2016;173:52–8.
[9] The World Bank. World Development Indicators (WDI); 2016. <http://datacatalogworldbankorg/>.
[10] Ranjan M, Jain V. Modelling of electrical energy consumption in Delhi. Energy 1999;24:351–61.
[11] Tso GK, Yau KK. Predicting electricity energy consumption: a comparison of regression analysis, decision tree and neural networks. Energy 2007;32:1761–8.
[12] Huang M, He Y, Cen H. Predictive analysis on electric-power supply and demand in China. Renew Energy 2007;32:1165–74.
[13] Wang W, Mu H, Kang X, Song R, Ning Y. Changes in industrial electricity consumption in China from 1998 to 2007. Energy Policy 2010;38:3684–90.
[14] Bianco V, Manca O, Nardini S. Electricity consumption forecasting in Italy using linear regression models. Energy 2009;34:1413–21.
[15] Bildirici ME, Bakirtas T, Kayikci F. Economic growth and electricity consumption: auto regressive distributed lag analysis. J Energy Southern Africa 2012;23:29–45.
[16] Shi K, Chen Y, Yu B, Xu T, Chen Z, Liu R, et al. Modeling spatiotemporal CO_2 (carbon dioxide) emission dynamics in China from DMSP-OLS nighttime stable light data using panel data analysis. Appl Energy 2016;168:523–33.
[17] Shi K, Yu B, Huang Y, Hu Y, Yin B, Chen Z, et al. Evaluating the ability of NPP-VIIRS nighttime light data to estimate the gross domestic product and the electric power consumption of China at multiple scales: a comparison with DMSP-OLS data. Remote Sens 2014;6:1705–24.
[18] Shi K, Yu B, Hu Y, Huang C, Chen Y, Huang Y, et al. Modeling and mapping total freight traffic in China using NPP-VIIRS nighttime light composite data. GISci Remote Sens 2015;52:274–89.
[19] Wu J, Wang Z, Li W, Peng J. Exploring factors affecting the relationship between light consumption and GDP based on DMSP/OLS nighttime satellite imagery. Remote Sens Environ 2013;134:111–9.
[20] Shi K, Huang C, Yu B, Yin B, Huang Y, Wu J. Evaluation of NPP-VIIRS night-time light composite data for extracting built-up urban areas. Remote Sens Lett 2014;5:358–66.

[21] Yu B, Shu S, Liu H, Song W, Wu J, Wang L, et al. Object-based spatial cluster analysis of urban landscape pattern using nighttime light satellite images: a case study of China. Int J Geograph Inform Sci 2014;28:2328–55.
[22] Lu H, Liu G. Spatial effects of carbon dioxide emissions from residential energy consumption: a county-level study using enhanced nocturnal lighting. Appl Energy 2014;131:297–306.
[23] Shi K, Chen Y, Yu B, Xu T, Li L, Huang C, et al. Urban expansion and agricultural land loss in China: a multiscale perspective. Sustainability 2016;8:790. doi: http://dx.doi.org/10.3390/su8080790.
[24] Yu B, Shi K, Hu Y, Huang C, Chen Z, Wu J. Poverty evaluation using NPP-VIIRS nighttime light composite data at the county level in China. IEEE J Sel Top Appl Earth Observ Remote Sens 2015;8:1217–29.
[25] Chen Z, Yu B, Hu Y, Huang C, Shi K, Wu J. Estimating house vacancy rate in metropolitan areas using NPP-VIIRS nighttime light composite data. IEEE J Sel Top Appl Earth Observ Remote Sens 2015;8:2188–97.
[26] Elvidge CD, Baugh KE, Kihn EA, Kroehl HW, Davis ER. Mapping city lights with nighttime data from the DMSP Operational Linescan System. Photogram Eng Remote Sens 1997;63:727–34.
[27] Elvidge CD, Baugh KE, Kihn EA, Kroehl HW, Davis ER, Davis CW. Relation between satellite observed visible-near infrared emissions, population, economic activity and electric power consumption. Int J Remote Sens 1997;18:1373–9.
[28] Xie Y, Weng Q. World energy consumption pattern as revealed by DMSP-OLS nighttime light imagery. GISci Remote Sens 2015:1–18.
[29] Amaral S, Câmara G, Monteiro AMV, Quintanilha JA, Elvidge CD. Estimating population and energy consumption in Brazilian Amazonia using DMSP night-time satellite data. Comput Environ Urban Syst 2005;29:179–95.
[30] Lo C. Urban indicators of China from radiance-calibrated digital DMSP-OLS nighttime images. Ann Assoc Am Geogr 2002;92:225–40.
[31] Townsend AC, Bruce DA. The use of night-time lights satellite imagery as a measure of Australia's regional electricity consumption and population distribution. Int J Remote Sens 2010;31:4459–80.
[32] Chand TK, Badarinath K, Elvidge C, Tuttle B. Spatial characterization of electrical power consumption patterns over India using temporal DMSP-OLS night-time satellite data. Int J Remote Sens 2009;30:647–61.
[33] He C, Ma Q, Liu Z, Zhang Q. Modeling the spatiotemporal dynamics of electric power consumption in Mainland China using saturation corrected DMSP/OLS nighttime stable light data. Int J Dig Earth 2013;6:1–22.
[34] Xie Y, Weng Q. Detecting urban-scale dynamics of electricity consumption at Chinese cities using time-series DMSP-OLS (Defense Meteorological Satellite Program-Operational Linescan System) nighttime light imageries. Energy 2016;100:177–89.
[35] Cao Z, Wu Z, Kuang Y, Huang N, Wang M. Coupling an intercalibration of radiance-calibrated nighttime light images and land use/cover data for modeling and analyzing the distribution of GDP in Guangdong, China. Sustainability 2016;8:108. doi: http://dx.doi.org/10.3390/su8020108.
[36] Elvidge CD, Baugh KE, Dietz JB, Bland T, Sutton PC, Kroehl HW. Radiance calibration of DMSP-OLS low-light imaging data of human settlements. Remote Sens Environ 1999;68:77–88.
[37] Liu Z, He C, Zhang Q, Huang Q, Yang Y. Extracting the dynamics of urban expansion in China using DMSP-OLS nighttime light data from 1992 to 2008. Landscape Urban Plan 2012;106:62–72.
[38] Zhao N, Zhou Y, Samson EL. Correcting incompatible DN values and geometric errors in nighttime lights time-series images. IEEE Trans Geosci Remote Sens 2015;53:2039–49.
[39] Meng L, Graus W, Worrell E, Huang B. Estimating CO_2 (carbon dioxide) emissions at urban scales by DMSP/OLS (Defense Meteorological Satellite Program's Operational Linescan System) nighttime light imagery: methodological challenges and a case study for China. Energy 2014;71:468–78.
[40] Elvidge CD, Ziskin D, Baugh KE, Tuttle BT, Ghosh T, Pack DW, et al. A fifteen year record of global natural gas flaring derived from satellite data. Energies 2009;2:595–622.
[41] Letu H, Hara M, Tana G, Nishio F. A saturated light correction method for DMSP/OLS nighttime satellite imagery. IEEE Trans Geosci Remote Sens 2012;50:389–96.
[42] Wu J, He S, Peng J, Li W, Zhong X. Intercalibration of DMSP-OLS night-time light data by the invariant region method. Int J Remote Sens 2013;34:7356–68.
[43] Zhang Q, Seto KC. Mapping urbanization dynamics at regional and global scales using multi-temporal DMSP/OLS nighttime light data. Remote Sens Environ 2011;115:2320–9.
[44] He C, Shi P, Li J, Chen J, Pan Y, Li J, et al. Restoring urbanization process in China in the 1990s by using non-radiance-calibrated DMSP/OLS nighttime light imagery and statistical data. Chin Sci Bull 2006;51:1614–20.
[45] Letu H, Hara M, Yagi H, Naoki K, Tana G, Nishio F, et al. Estimating energy consumption from night-time DMPS/OLS imagery after correcting for saturation effects. Int J Remote Sens 2010;31:4443–58.
[46] Lo C. Modeling the population of China using DMSP operational linescan system nighttime data. Photogram Eng Remote Sens 2001;67:1037–47.
[47] Xie H, Zou J, Peng X. Spatial-temporal difference analysis of cultivated land use intensity based on emergy in Poyang Lake Eco-economic Zone. Acta Geogr Sinica 2012;67:889–902.
[48] Brewer CA, Pickle L. Evaluation of methods for classifying epidemiological data on choropleth maps in series. Ann Assoc Am Geogr 2002;92:662–81.